SIMULATING BIO-COMPOSITE CYCLING HELMET PERFORMANCE THROUGH FEA AND CFD APPROACHES

Mohd Naim Abdullah, F. Mustapha, M. K. H Muda, M. K. A. Arrifin, A. S. M. Rafie, M. A. Shamsudin

Department of Aerospace, Faculty of Engineering,
Universiti Putra Malaysia,
43400 Serdang, Selangor, Malaysia

Abstract

Finite Element Analysis (FEA) and Computational Fluid Dynamics (CFD) analysis were performed in this work in order to obtain the best design for safety and aerodynamic performance of the bicycle cycling helmet. FEA analysis was computed on two different helmet designs to determine the critical area subjected to impact. A pressure load was applied on the helmets' outer surface to simulate oblique loading. The critical areas of the helmets were then highlighted and identified, enabling design improvements to be made on both designs. CFD analysis was then executed in order to obtain the lowest drag coefficient number in reducing the air resistance induced by both of the helmet designs, inherently increasing cyclist performance and ensuring competition success.

Keywords: Bio-composite cycling helmet, cycling helmet performance, Finite Element Analysis (FEA), Computational Fluid Dynamics (CFD)

Introduction

Sports engineers are individuals who conduct studies in design and build new equipment based on the requirements of athletes. According to Taha, Hassan, Abdul Majeed, Aris, and Sahim (2013), sports engineers gauge the behaviour of equipment, athletes and their interactions in a controlled environment. Additionally, they also model the forces acting on athletes and their equipment via Finite Element Analysis (FEA) or simulate the airflow around equipment through Computational Fluid Dynamics (CFD) (Taha et al., 2013). Helmets are essential for reducing injuries to the rider's head when accidents occur. It is imperative that the helmet be designed perfectly in order to increase safety performance without reducing the rider's speed, while remaining comfortable to the user (Alam et al., 2010). In a sport cycling competition, winning is the first priority and hence all supporting equipment must have a special design for the specific purpose of winning competitions. In bicycle racing, air resistance is the main factor to be considered, as well as the design of the outer finishing surface of the helmet. Safety and performance cannot be avoided in the making of a robust bicycle helmet design. In

order to reduce development costs, FEA and CFD analysis are often used to obtain an initial view of the product before starting production.

The finite element method (FEM) is a numerical technique for finding approximate solutions to partial differential equations (PDE) as well as integral equations. Felippa (2004) states that FEM was developed initially and prospered as a computer-based simulation method for the analysis of aerospace structures (Felippa, 2004). The method then found its way into both the design and analysis of complex structural systems, and began to be applied not only in Aerospace Engineering but also in Civil and Mechanical Engineering. According to Douglas, Gasiorek, and Swaffield (2001), FEM was initially developed for structural analysis but then became utilized for fluid flow predictions as it offers the advantage of a non-regular grid (Douglas et al., 2004). This allows FEM simulations to address complex boundary geometries. The finite volume method draws together the best attributes of FDM and FEM in that it is capable of simulating complex boundary geometries and accurately modeling conservation for each cell, while at the same time utilizing relatively straightforward finite difference relationships to represent governing differential equations. The ability to seek the numerical solutions of these governing equations under a given set of boundary and initial conditions led to the development of computational fluid dynamics (CFD).

CFD is one of the branches of fluid mechanics that uses numerical methods and algorithms to solve and analyze problems involving fluid flows. There are millions of calculations required for simulating the interaction of fluids and gases with complex surfaces. These calculations are handled by computers. Douglas et al. (2001) explains that a CFD code has three basic components: a pre-processor, a solver and a post-processor (Douglas et al., 2001). The solver is the heart of the code, carrying out the major computations and providing numerical solutions. The pre-processor and post-processor are at the front and end of the code, providing the user/machine interface that allows a CFD operator to communicate with the solver, inputting data to define the problem to be simulated, commanding the solver to use certain models and schemes to carry out the simulation, and, finally, presenting the computed results for study. Apart from these key elements, a commercial package aimed at multi-purpose modeling will have a suite of models for various flow problems, such as various turbulence models to cover a range of turbulence conditions and assumptions. The package should also have a library of material properties for defining the fluid media and solid boundaries in the computational domain. Experience is expected to guide the user in the choice of appropriate model and boundary conditions.

The kenaf plant (*Hibiscus cannabinus*) contains fiber in its bark and core. The stems contain lobes for the base area and decline in number when reaching the top of the kenaf plant. The bark contains a long fiber known as bast fiber and a woody core comprising of short core fibers (Charles, Julia, & John, 1998). Kenaf fibre (KF) has been mixed with other composites such as polypropylene (PP), thermoplastic natural rubber (TPNR), polypropylene/ethylene-propylene-diene-monomer (PP/EPDM), and maleic anhydride polypropylene (MAPP). Research conducted by Anuar and Zuraida (2010) indicates that each mixture will produce a different outcome in terms of tensile, flexural and impact result (Anuar & Zuraida, 2010).

Mixing TPNR-kenaf-MAPP only slightly increases impact strength compared to a mixture of just TPNR-kenaf. However, impact strength increases drastically with the mixture PP/EPDM-kenaf-MAPP. This shows that impact strength can be increased with a certain mixture of kenaf fibre. TPNR and PP/EPDM can be produced via the double melt blending method using a Haake internal mixer before they are compression moulded. Kenaf fibres are also suitable to be combined with poly-L-lactic acid (PPLA) resin in order to improve their mechanical properties. A study by Nishino, Hirao, Kotera, Nakamae, and Inagaki (2003) reported that the young modulus and tensile strength can be improved up to 6.3 GPa and 62 MPa respectively, with a fibre content of 70 vol% (Nishino et al., 2003).

In this paper, kenaf fibre will be the main material used for inputting the required data in FEA and CFD computations in order to investigate preliminary design strategies for a sport cycling helmet, with the objective of improving aerodynamic performance and oblique loading.

Finite Element Analysis (FEA)

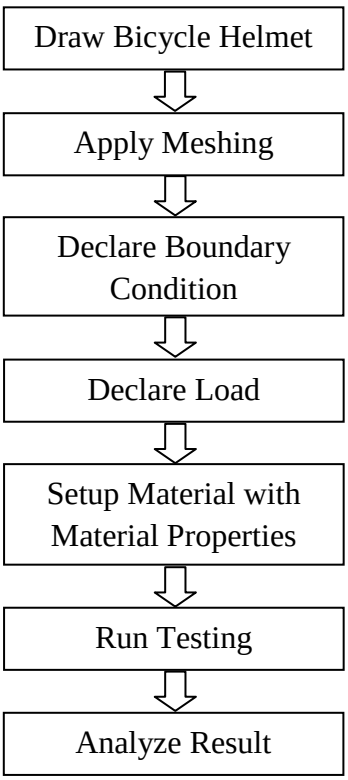

Figure 1: Flow Chart of FEA analysis process.

The 3D drawing for the proposed sport cycling helmet was executed using CAD software and the dimensions were based on the standard size of a bicycle helmet. The dimension reference was just for the basic area, which is a sizing pad that follows the

adult head circumference as stated in Mills and Gilchrist (2008). In the first stage of the FEA analysis, the material property of the bicycle helmet was chosen and input into the user defined features available in the FEA software. Kenaf fiber was the main material used for this work. Static force was applied to the helmet model as a main loading to simulate oblique loading occurring on the helmet. 6kN of force was chosen according to the ideal value reported in Mills and Gilchrist (2008) for oblique loading simulations. In this paper, the force absorption for the oblique impact of a 6kN force during the actual impact test was equivalent to 5.4m/s velocity.

This paper proposes two initial design concepts. The first design has air ventilation at the top surface and the second design incorporates a full stream lining aerodynamics concept without air ventilation (Figure 2 and Figure 3 respectively). FEA analysis was applied to these two designs by using FEA software to compute the different points of maximum stress.

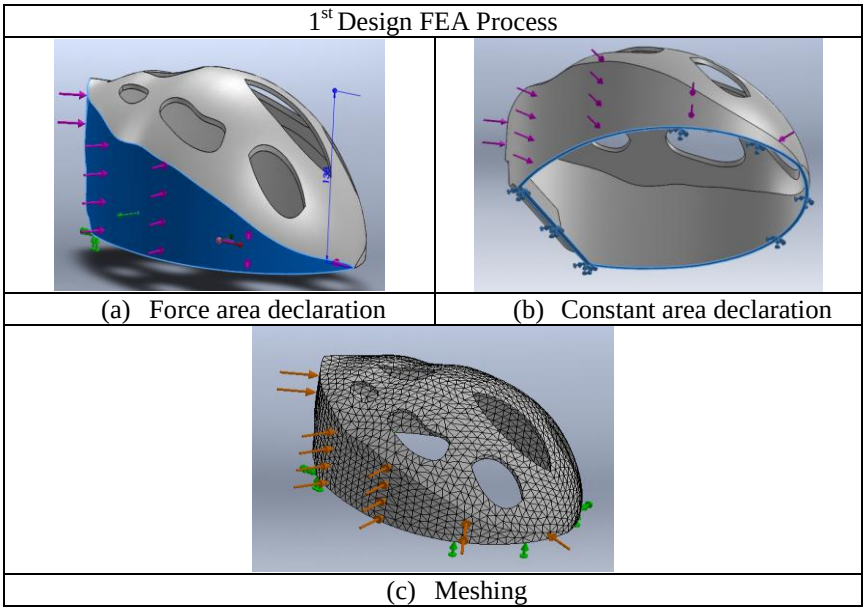

Figure 2: FEA process of the first design.

Figure 2 (a) shows the force area that was applied to the side of the helmets' surface where a 6kN force was distributed constantly along the highlighted area's surface. The meshing view is shown in Figure 2 (b) where the meshing process was executed in default mode and the model in hex mode.

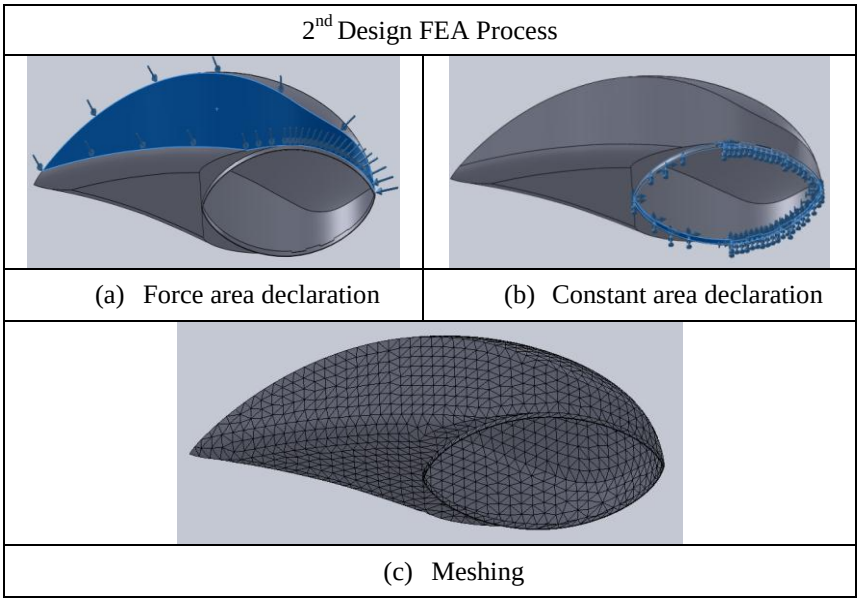

Figure 3: FEA process of the second design.

The FEA process was repeated for the second design concept, starting from force area declaration, continuing with fix area declaration, and concluding with the meshing process. The force area is shown in Figure 3 (highlighted in blue). The blue arrows show the direction of force that is perpendicular to the surface. This surface represents the impact area of the helmet when touching the road surface in actual conditions. The constant area refers to the area that is mounted to the user's head using a strap. Meshing settings were set at normal density to minimize the time taken for analysis.

For the material properties, the kenaf yield strength was 25 MPa as defined by Nishino, Hirao, and Kotera (2006). The density value was 1.193 g/cm^3. Amel, Paridah, Sudin, Anwar, & Hussein (2013) have reported that the effect of the fiber extraction method of kenaf base fibre is predominantly consistent, and this finding was supported by Nishino et al. (2006). All of this data was used as baseline and reference data for computing the FEA of the designs in this study.

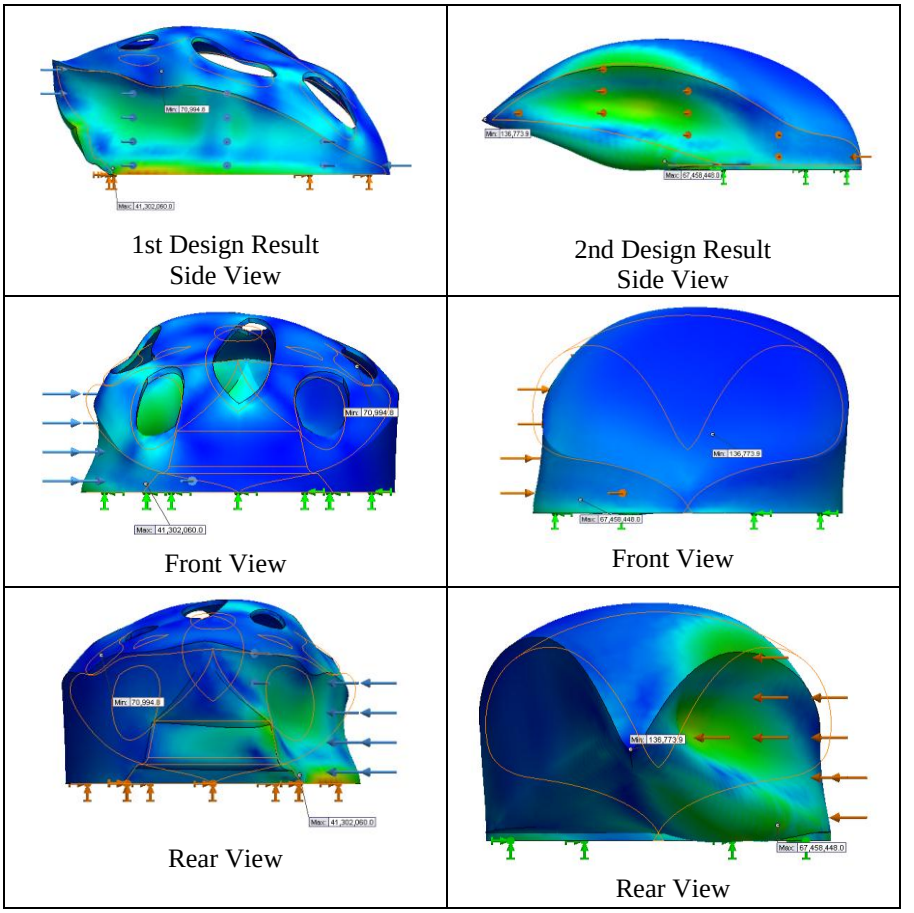

Figure 4: Comparison of First and Second Design in FEA analysis result.

As the results indicate, these two designs have a different critical point even with the same force and thickness applied. This shows that changing the helmet design can alter the maximum stress value. The design was therefore improved to reduce the impact absorbed by the helmet and the injury to the cyclist's head (Figure 4). The red color located at the centre of the helmet indicates the highest stress absorbed by the helmet. The results indicate that the shape of the helmet in the second design was affected as it bent to the other side of the impact force. The same results apply to the first design where the original shape also changed, as illustrated in Figure 4. The critical point was located at the side of the head circumference for both designs.

Internal structure was then added to increase the strength of the helmet to withstand a 6kN force of oblique impact, in order to minimize injury to the cyclist's head. This modification was also intended to prevent substantial changes to the original shape of the helmet.

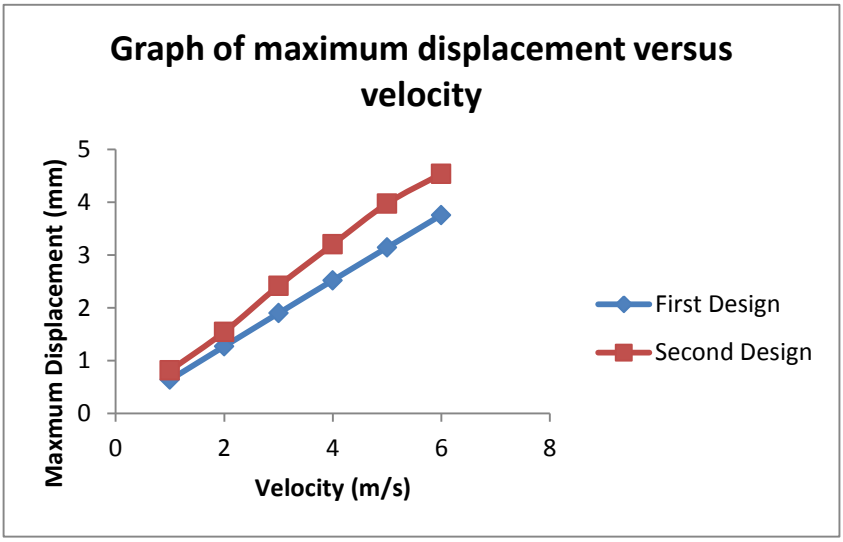

Figure 5: Graph of maximum displacement compared to the original shape versus velocity of impact.

From Figure 5, it is clearly demonstrated that the maximum displacement of the second design was larger than the first design. Different helmet shapes and patterns will give different displacement results at certain points on the helmet's surface even if the speed of impact is same. The location of the maximum displacement was also different between the two designs, as the first design's maximum displacement was located at the rear of the pad lining while the second design's displacement was located at the front of the pad lining. However, the maximum displacement of both helmets was located far away from the impact point, which means the maximum displacement was not directed towards the cyclist's helmet. The displacement also increased parallel to the increase of the impact speed.

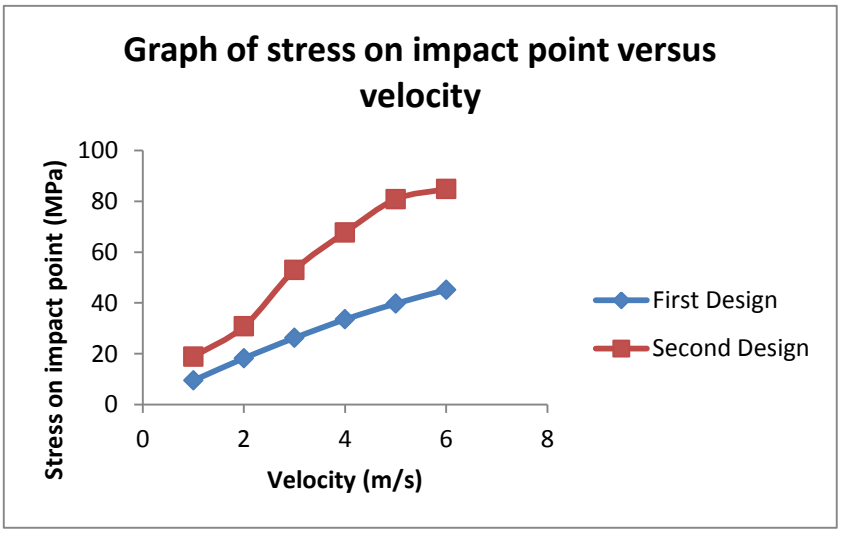

Figure 6: Graph of stress on impact location point versus velocity of impact.

Figure 6 shows the graph of stress on the main impact point versus velocity of impact. This graph shows the different stresses received by both helmet designs on the main location of the impact. The main impact point refers to the part of the helmets' surface that first touched the road surface.

The stress of impact on this specific point was higher for the second design compared to the first design, as illustrated in Figure 6. However, the stress for the second design was located at the extra length on the helmet's rear area. This was a hollow location far away from the cyclist's head position since the second helmet is longer than the normal human head. The extra length was incorporated for aerodynamic purposes. In this impact analysis, the second design proved better than the first design since it relocated the maximum impact point away from the lining of the pad area, which was the area directly in contact with the cyclist's head. It therefore can be concluded that the second helmet design performs better in impact testing as it distributes stress along the helmet surface.

Computational Fluid Dynamic

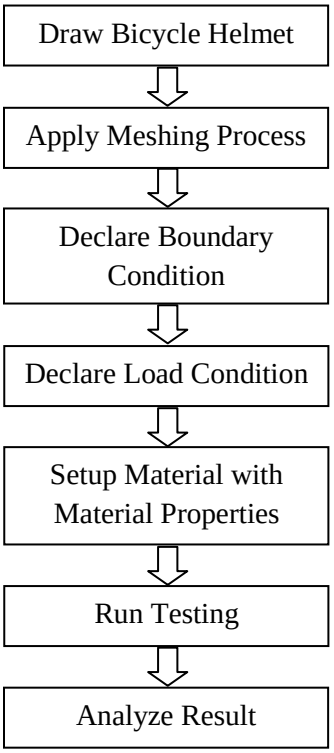

Figure 7: Flow Chart of CFD analysis process.

Using the same 3D drawing as in the FEA analysis, CFD analysis was performed to investigate the air flow created by the two designs. However, some simple modifications were made to the 3D drawing in order to create the CFD internal testing area.

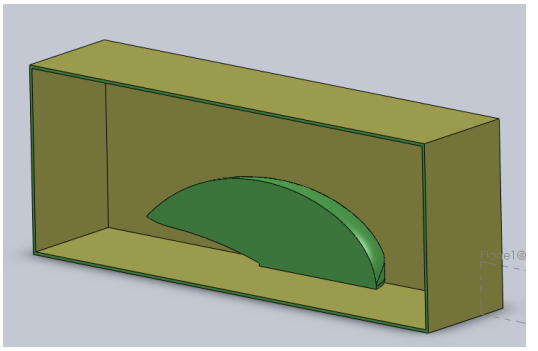

Figure 8: Part of the helmet surface in an analysis area.

Figure 8 shows the box area depicting one side of the bicycle helmet. The green color represents the bicycle helmet and the yellow color represents the box that was used as a 'wind tunnel' testing area.

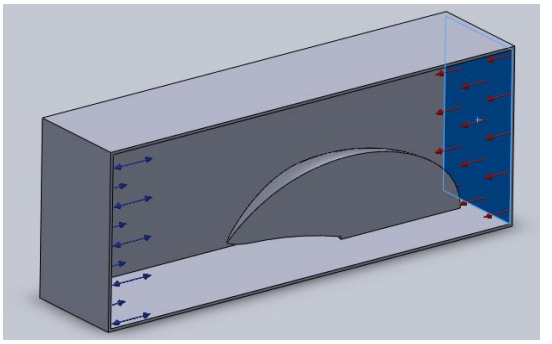

Figure 9: Inlet and outlet area of the air flow.

Figure 9 shows the inlet and outlet areas for the air flow inside the box with the same direction as in the figure. The volume flow rate was set at 8.33 m^3/s and the environment pressure was same as the atmosphere pressure, which was 101325 Pa. The temperature value was 301K.

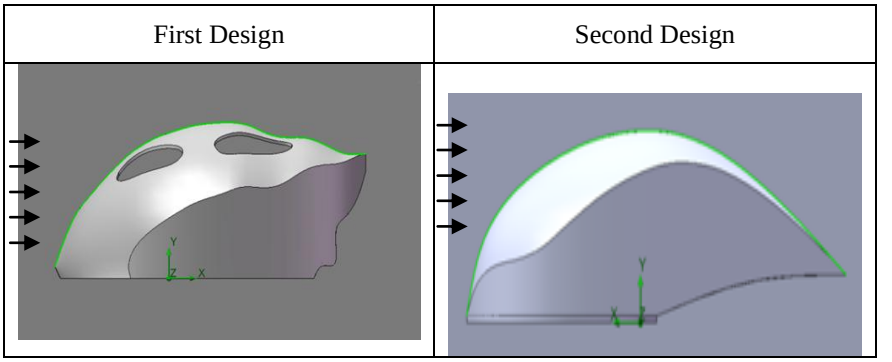

Figure 10: Location of point line taken for CFD analysis.

Figure 10 shows the points taken along the path line in green color. The line was located at the center top surface of the helmet. The points were taken randomly with very small distance between each point, starting from the front area up till the rear end. The air flow was from left to right as shown by the arrow directions.

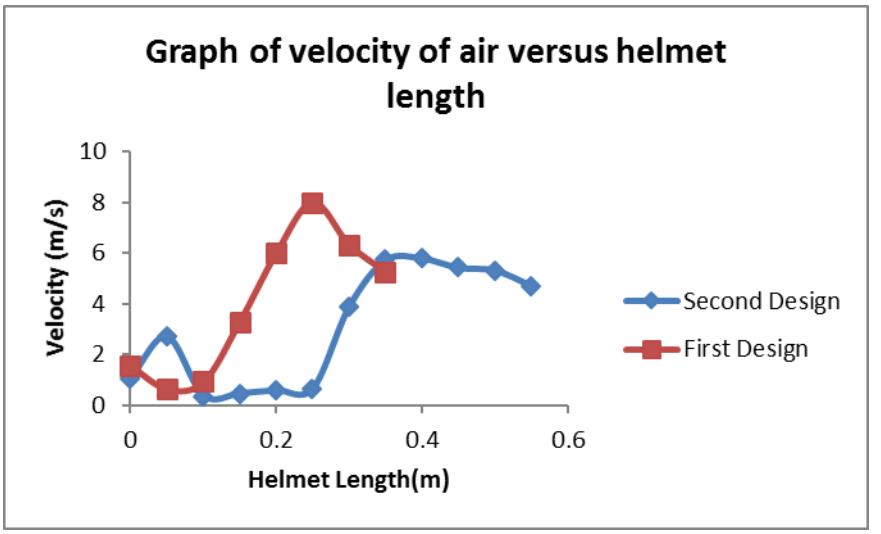

Figure 11: Graph of velocity of air versus helmet length.

Figure 11 shows the different velocities of various points on the upper surface of the two helmet designs. The points were recorded starting from the front area of the helmets' upper surface up to the rear. They were of different lengths since the second helmet design was longer than the first design. The points were recorded every 0.05m.

Air velocity was constant for air inlet velocity, which is 8.33m/s. As illustrated in Figure 11, the starting velocity was not same for both designs as the first design showed a velocity drop at the starting area (the front area of the helmet) while the second design did not. This means that the second design is more aerodynamic as the air velocity increased immediately upon touching the helmet's front surface.

From the graph, it can be seen that the air velocity increased at the helmets' half length for both the designs, since their curves are not very different. However, a greater velocity drop was recorded in the first design compared to the second design. This means that the second design is superior in avoiding the velocity drop, which affects air resistance and slows down the cyclist's speed.

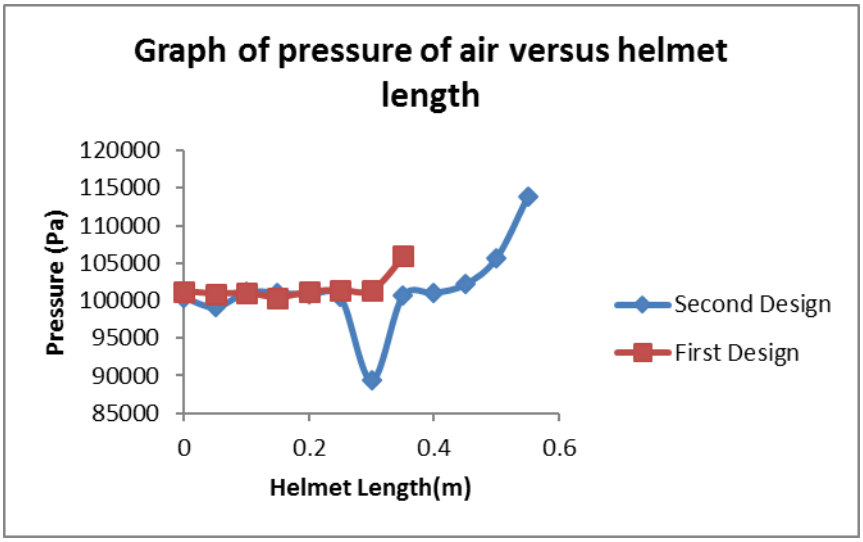

Figure 12: Graph of air pressure versus helmet length.

Figure 12 shows that there was not much difference in the air pressure of the two designs at the start of the air touching the helmets' front area. The results of the first design showed that pressure was maintained for the whole body with only a slight increase in the rear area. The second design, on the other hand, showed a dramatic drop in pressure in the middle of the helmet's body.

According to the airfoil concept, when pressure on the upper surface is low, the lift force will increase. This reduces the weight of the cyclist while simultaneously increasing the cyclist's speed. In the second design, the pressure started to increase at the rear end of the helmet's body, thus increasing the downward force. However, it should be noted that this would not directly affect the cyclist's weight since that area is located on the extra length of the helmet.

1st Design Result	2nd Design Result
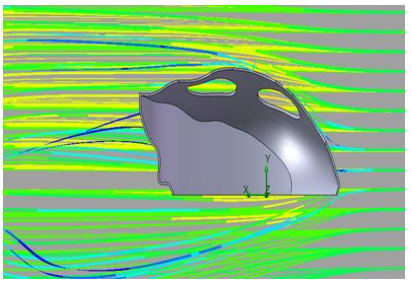	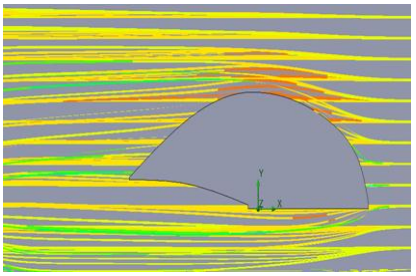
Side View	Side View
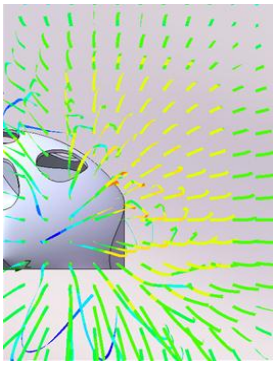	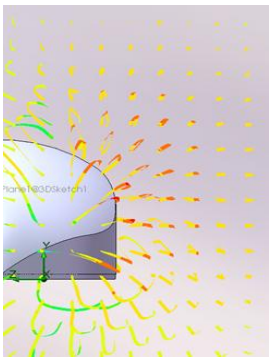
Front View	Front View
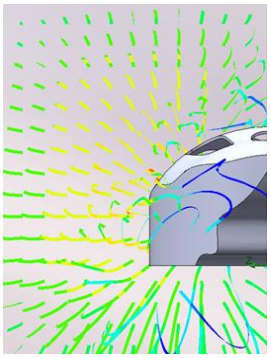	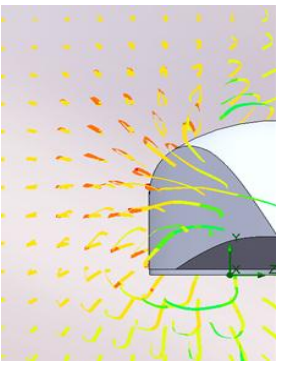
Rear View	Rear View

Figure 13: Comparison of First and Second Design in FEA analysis result.

Figure 13 shows the different patterns of the streamline for the two bicycle helmet designs. The line is straighter after going through the helmet surface for the second design compared to the first design. There was also no vortex occurring in the second design. Furthermore, air flow lines were not really split after going through the helmet surface, unlike in the first design.

1st Design Result	2nd Design Result
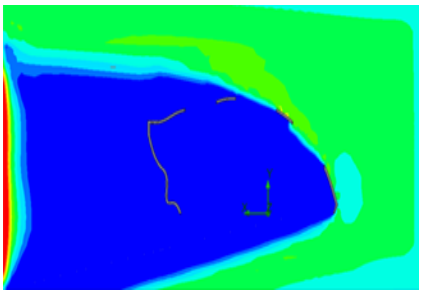	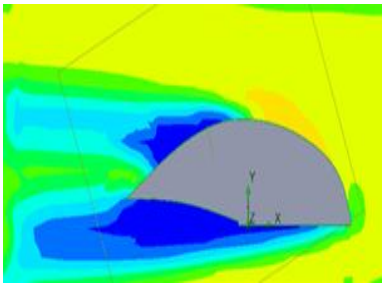
Side View	Side View

Figure 14: Comparison of the First and Second Design in FEA analysis result for contour view.

Figure 14 shows the different contour views of the two helmet designs in terms of velocity parameters. The first design clearly shows a large zero velocity area at the back area of the helmet. This would negatively affect the speed of the cyclist because it would cause considerable air resistance. As for the second design concept, only a small zero velocity deviation was detected in the top back area as compared to the first design. This clearly highlights that the second design possesses less air resistance, since there was less drop in its velocity. Less change in air velocity inherently smoothens the cruise of the cyclist.

Conclusion

The results generated by the second design contribute towards reducing the total air resistance of the cyclist while racing. The second design was therefore selected for further investigation of its effect on impact and air resistance when using kenaf fibre as the core material. An internal frame structure will be added to reinforce the helmet's structure while increasing the time of fraction. This time increase will reduce the force absorbed by the helmet while simultaneously reducing the impact on the cyclist's head. According to the CFD analysis's results, the air flow line pattern was steadier in the second design of the helmet compared to the first design. This indicates that the air resistance is less in the second design. This situation was clearly demonstrated in the contour view, where there were big areas of lower air velocity (indicated in blue) that covered the back area of the first helmet design. This air velocity drop was reduced in the second design, as shown in Figure 13.

From both analyses, it was found that the maximum force and critical point could be changed parallel to the changing of the helmet design. Playing with the design will give better output in line with the objective of this project, which is to reduce the force of impact absorbed from collisions.

In conclusion, it can be surmised that the second design is superior to the first design, since in the impact analysis, the critical stress point of the second design was located

away from the pad lining. The stress distribution of the second design also focused on the rear hollow area, which is located away from the cyclist's head. These results can reduce the direct impact on the cyclist's head in the event of a collision.

Acknowledgements

This research is supported by a grant from Universiti Putra Malaysia. Special thanks to UPM Aerospace Laboratory department for providing wind tunnel equipment.

References

B. Ahmed Amel, M. Tahir Paridah, R. Sudin, U.M.K. Anwar, Ahmad S. Hussein. (2013). Effect of fiber extraction methods on some properties of kenaf bast fiber. *Industrial Crops and Product, 46,* 117 – 123.

Carlos A. Felippa, (Last Updated Fall 2004). *Introduction to finite element method*. Department of Aerospace Engineering Sciences and Centre for Aerospace Structures University of Colorado Boulder, Colorado 80309 – 0429, USA. Retrieve on 1st October 2008.

Charles L. Webber III, Julia Whitworth, John Dole. (1998). Kenaf (Hibiscus Cannabinus L.) core as a containerized growth medium component. *Industrial Crops and Product, 10,* 97 – 105.

Firoz Alam, Harun Chowdhury, Zakaria Elmir, Andika Sayogo, James Love, Aleksandar Subic. (2010). An experimental study of thermal comfort and aerodynamic efficiency of recreational and racing bicycle helmets. *Procedia Engineering, 2,* 2413 – 2418.

H. Anuar, A. Zuraida. (2010). Improvement in mechanical properties of reinforced thermoplastic elastomer composite with kenaf bast fibre. *Part B, 42,* 462 – 465.

John F. Douglas, Janusz M. Gasiorek, John A. Swaffield. (2001). Fluid Mechanics (4th ed.). (pp. 89 – 167). Pearson Prentice Hall.

Mohd Suhairil Meon, Muhamad Fauzi Othman, Hazran Husain, Muhammad Fairuz Remeli, Mohd Syahar Mohd Syawal. (2012). Improving tensile properties of kenaf fibers treated with sodium hydroxide. *Procedia Engineering, 41,* 1587 – 1592.

N. J. Mills, & A. Gilchrist. (2008). Oblique Impact Testing of Bicycle Helmets. *International Journal of Impact Engineering, 35,* 1075 -1086.

Takashi Nishino, Koichi Hirao, Masaru Kotera, Katsuhiko Nakamae, Hiroshi Inagaki. (2003). Kenaf reinforced biodegradable composite. *Composite Science and Technology, 63,* 1281 – 1286.

Takashi Nishino, Koichi Hirao, Masaru Kotera. (2006). X-ray diffraction studies on stress transfer of kenaf reinforced poly (L-lactic acid) composite. *Part A, 37,* 2269 – 2273.

Zahari Taha, Mohd Hasnun Arif Hassan, Anwar P.P. Abdul Majeed, Mohd Azri Aris, Nina Nadia Sahim. (2013). An Overview of Sports Engineering: History, Impact and Research. *Movement, Health & Exercise, 2,* 1-14.